Theoretical Study of Toluene Adsorbed on Zeolites X and Y: Calculation of ^{13}C NMR Parameters

Alexandra Simperler,[†] Robert G. Bell,*[,†] Andreas Philippou,[‡] and Michael W. Anderson[‡]

Davy Faraday Research Laboratory, The Royal Institution of Great Britain, 21 Albemarle Street, London W1S 4BS, United Kingdom, and UMIST Centre for Microporous Materials, Department of Chemistry, UMIST, P.O. Box 88, Manchester M60 1QD, United Kingdom

Received: March 18, 2002; In Final Form: July 18, 2002

The adsorption of toluene on basic faujasite-type zeolites with different Si/Al ratio and charge compensating interstitial alkali metal cations, M−X and M−Y (M = Li^+, Na^+, K^+, Rb^+, and Cs^+) has been investigated with molecular mechanics and quantum chemical methods. The Monte Carlo docking method was used to find energetically favorable positions of the toluene molecule within the zeolitic void space. Subsequently, density functional calculations of geometries, Mulliken partial charges, adsorption energies, and ^{13}C NMR chemical shift parameters of clusters representing the adsorption site were performed. The polarization of the toluene carbon atoms is held to be a decisive step in the zeolite-catalyzed alkylation reaction and will therefore influence the outcome of this reaction in terms of the preference between ring and side-chain alkylation. Both the Lewis acidity of the alkali metal cations and, to a lesser extent, the basicity of the zeolite, which is governed by the nature of these interstitial cations and by the amount of aluminum atoms in the framework, simultaneously influence the electron distribution within the toluene molecule. Key geometric parameters, the Mulliken partial charges of the toluene carbon atoms, adsorption energies, and the chemical shift parameters are presented as a function both of the alkali cation and of the Al/Si ratio of the zeolite. As a general result, the ^{13}C NMR chemical shift parameters δ_{11}, δ_{22}, δ_{33}, δ_{aniso}, and η of the toluene carbon atoms are sensitive to the changes in composition mentioned above, while δ_{iso} hardly shows any sensitivity. Our results are in accord with experimental findings and indicate that adsorption on a single alkali cation site in zeolite X or Y does not result in the activation of toluene for alkylation. We expect our results to be useful in improving and interpreting data from MAS NMR experiments.

1. Introduction

The side-chain or ring alkylation or both of toluene with methanol catalyzed by zeolites lead to a variety of products of industrial importance. Hence, this reaction has been the subject of several experimental and theoretical studies,[1−14] which have aimed to shed light on the reaction mechanism. The use of zeolites as catalysts for this type of reaction allows very effective control over the outcome/yield of certain products and moreover constitutes a more environmentally benign process than traditional Friedel−Crafts alkylation. Depending upon the acidity and pore size of the molecular sieve, ethylbenzene, styrene, or xylenes or a combination of these can be obtained as products. It is well-known that acid zeolites, such as H-ZSM5, favor ring alkylation whereas basic zeolites, principally alkali metal-containing faujasite-type zeolites X and Y,[15−16] favor side-chain alkylation. The basicity of zeolites X and Y is attributed to the Lewis basic framework oxygen atoms. This basic character of the zeolite increases with the number of framework aluminum atoms occupying tetravalent T sites (and hence with the number of charge-compensating cations) and also with the identity of the cations themselves, with the base strength decreasing in the order $Cs^+ > Rb^+ > K^+ > Na^+ > Li^+$. According to the currently accepted mechanism first proposed by Itoh et al.,[14] the first elementary step for side-chain alkylation in basic zeolites is the dehydrogenation of methanol to form an active species such as formaldehyde, formate, or surface-adsorbed species, in which the carbon atom becomes positively polarized. This particular step has been widely discussed in the literature.[1,3,4,6,8,17] However, in the present work, our main focus will be on the adsorption of toluene in faujasite-type zeolites in the absence of methanol. Two main factors seem to influence the electron distribution within the toluene molecule. First, there is the fairly strong interaction of the Lewis acidic extraframework cation with the π-electron system of the aromatic toluene ring. Second, there is the interaction between the toluene methyl hydrogen atoms and the basic framework oxygen atoms. The latter results in the elongation of one of the methyl C−H bonds interacting with the framework oxygen atoms and in a negative polarization of the methyl carbon. The positively polarized carbon of the reactive species derived from methanol attacks at the negatively polarized methyl carbon of toluene (electrophilic substitution). Finally, styrene may further be hydrogenated by H_2 (produced during the methanol dehydrogenation) to ethylbenzene.

In this paper, we investigate the adsorption of toluene in basic zeolites X and Y with molecular mechanics and quantum chemical methods. Our main intention is to determine how five different interstitial alkali metal cations and the basic catalyst environment influence the electronic structure of the aromatic molecule. A Monte Carlo docking procedure revealed the six-

* To whom correspondence should be addressed. Fax: +44 20 7629 3569. E-mail: rob@ri.ac.uk.
[†] The Royal Institution of Great Britain.
[‡] UMIST Centre for Microporous Materials.

10.1021/jp0257799 CCC: $22.00
Published on Web 09/26/2002

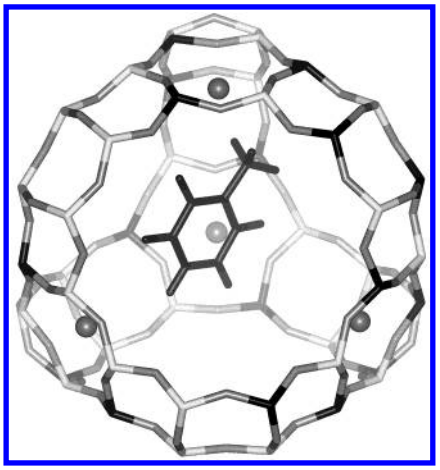

Figure 1. Stylized drawing of toluene (black) in the large cavity of a faujasite-type zeolite Na-Y as obtained by the Monte Carlo docking method. Within a typical minimum position, the toluene molecule is found to be above a six-ring of the sodalite cage unit (SII site).

ring window between the supercage and the sodalite cage, with an associated alkali cation at the SII position, as a strong adsorption site for toluene and, hence, an obvious location for the alkylation reaction to occur. Cluster models were selected to represent this active site of the catalyst and were studied with density functional methods. Through calculation of geometric parameters, Mulliken partial charges, adsorption energies, and ^{13}C NMR chemical shift parameters, the effects on toluene of varying the cation and zeolite framework composition were examined. The choice of clusters with alkali metal cations of different electronegativity (EN) and all possible Si/Al ratios cover the whole range of interactions within a real zeolite framework. Among the properties calculated, the ^{13}C NMR chemical shift parameters are especially sensitive to changes in the electron distribution of the molecule caused by variations in its environment. In particular, the principal components, δ_{11}, δ_{22}, and δ_{33}, together with the anisotropy parameter, δ_{aniso}, and the asymmetry factor, η, offer a richer and more sensitive characterization than the respective isotropic shift, δ_{iso}. By considering a broad portfolio of simulated properties, we thus may gain a more detailed insight into the type and strength of interactions that exist between catalyst and molecule at an early stage of the alkylation reaction.

2. Methods

The Monte Carlo docking[18] method was used to locate preferred adsorption sites of a single toluene molecule in zeolite Na-Y, which were taken as representative for all other zeolites under consideration. The *cff91_czeo* force field[19] was used in these calculations, which involved full flexible framework minimization calculations after the Monte Carlo insertion stage. The state of lowest energy was found to be with the ring plane of the toluene above an SII Na^+ cation, that is, toluene is situated in the faujasite supercage above the sodalite cage six-ring window, as shown in Figure 1. This result accords with neutron powder diffraction investigations by Klein et al.[20] of toluene in zeolite Na-Y and also with the simulation studies of Auerbach et al.[21] on the binding of benzene in Na-Y. We note that, for Na-X, the latter authors also predicted a binding site for benzene over the SIII cation site of similar energy to that of the SII cation site. Although we did not consider the effect of occupied SIII cation sites in our initial docking calculations, the results indicated that, for toluene, the region of the SIII site was sterically disfavored compared both to the SII and to the 12-membered window sites, most likely because of the greater curvature of the zeolite framework at this location and reduced possibility for van der Waals' contact. For the purposes of the current work, we therefore consider only the SII site for all Si/Al ratios. The aromatic toluene ring is located in front of the sodalite cage six-ring window of Na-Y with nearly parallel orientation of the aromatic ring plane to the plane of the six-ring window. From this configuration, reasonable molecular models representing the site of adsorption were selected, which comprised toluene, the cation M^+ ($M^+ = Li^+$, Na^+, K^+, Rb^+, and Cs^+), and the six-membered ring fragment with Si/Al ratios of 5, 2, and 1. Toluene alone, denoted as cluster **T**, and toluene + cation, cluster $\mathbf{T^{M^+}}$, were included in the study as well (see Figure 2) to investigate the influence of the cation alone on the aromatic molecule. The cluster $\mathbf{ZT^{I}}$ (Si/Al = 5) represents zeolite Y, whereas the other three clusters, $\mathbf{ZT^{IIm}}$ and $\mathbf{ZT^{IIp}}$ (both with Si/Al = 2) and $\mathbf{ZT^{III}}$ (Si/Al = 1) represent zeolite X. In the case of cluster $\mathbf{ZT^{II}}$, both possible relative positions of the two Al atoms, consistent with Löwenstein's rule,[22] were considered (i.e., meta ($\mathbf{ZT^{IIm}}$) and para ($\mathbf{ZT^{IIp}}$) configurations). We refer to the whole series as clusters **ZT**. We also calculated the corresponding clusters without the toluene molecule, referred to as clusters **Z** (comprising $\mathbf{Z^{I}}$, $\mathbf{Z^{IIm}}$, $\mathbf{Z^{IIp}}$, and $\mathbf{Z^{III}}$, see Figure 2). The nomenclature of the toluene carbon atoms is also

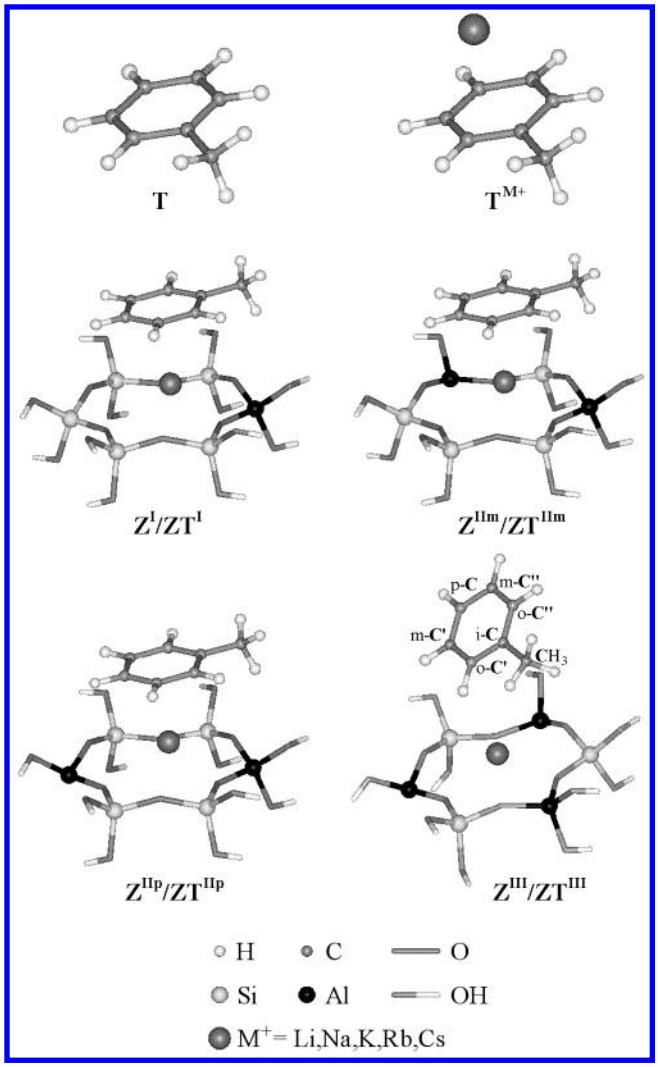

Figure 2. Molecular graphics of the cluster models used in this work: **T** (toluene); $\mathbf{T^{M^+}}$ (toluene + cation); **Z** (cation + zeolite fragment, representing the six-ring of the sodalite cage unit of faujasite); **ZT** (toluene + cation + zeolite fragment).

illustrated in Figure 2: methyl carbon (**C**H_3), ipso carbon (i-**C**), ortho carbon (o-**C**), meta carbon (m-**C**), and para carbon (p-**C**); ′ and ″ indicate o- and m-**C** on specific sides of the molecule.

The "dangling" bonds of the T-atoms of the fragments representing the zeolite were saturated with OH groups pointing away from the toluene molecule to avoid contributions from O−H···π-electron interactions. The charge of the cluster was kept at zero by saturating only one of the aluminum atoms with two OH and all of the others present with just one OH group. In our experience, the uncharged zeolite framework is best represented in this manner. After optimizing the positions of the terminating protons, we fixed all hydroxy groups to keep the nonring oxygen atoms at their crystallographic positions[15] to retain a reasonable representation of the zeolite framework. In subsequent optimizations, we allowed the zeolite ring atoms (in the absence of toluene but in the presence of the cation) to relax to obtain reasonable Si−O and Al−O bond lengths and to allow changes in the geometry of the six-membered ring due to the type of alkali cation, which was allowed to relax as well. In the final set of optimizations, toluene was added at the position determined by Monte Carlo docking, and both the aromatic molecule and the alkali metal cation were allowed to relax without any constraints but with the zeolite fragment fixed at the geometry calculated before. Quantum chemical calculations were performed at the PW91[23] level of theory and with the DNP basis set (i.e., a double numerical basis function together with polarization functions, comparable to the Gaussian basis set 6-31G(d,p)[24]) with the DMol programs.[25] The ^{13}C NMR shift parameters (δ_{iso}, δ_{11}, δ_{22}, δ_{33}, δ_{aniso}, η) were obtained from GIAO (gauge-independent atomic orbitals)[26,27] calculations at B3LYP[28] level (Gaussian 98 programs[29]) with 6-311++G(d,p)[30] basis set for C and H atoms and TZV[31] for all other atoms (except Rb and Cs, for which the SDD[32] basis set was used). All chemical shift parameters are referenced to tetramethylsilane (TMS) ($\sigma_{iso}(^{13}C) = 183.04$ ppm). The principal elements are denoted by δ_{11}, δ_{22}, and δ_{33}, where δ_{11} is the least-shielded element and δ_{33} is the most-shielded element ($\delta_{11} = \delta_{22} = \delta_{33}$). δ_{iso}, the isotropic chemical shift, is obtained via the well-known relation $\delta_{iso} = {}^1/_3(\delta_{11} + \delta_{22} + \delta_{33})$. The anisotropy parameter, δ_{aniso}, is the difference between the most-shielded component and the isotropic chemical shift, $\delta_{aniso} = \delta_{33} - \delta_{iso}$. The asymmetry factor, η, is defined by the following equations: $\eta = (\delta_{22} - \delta_{33})/(\delta_{11} - \delta_{iso})$ for $|\delta_{11} - \delta_{iso}| \geq |\delta_{33} - \delta_{iso}|$ and $\eta = (\delta_{22} - \delta_{11})/(\delta_{33} - \delta_{iso})$ for $|\delta_{11} - \delta_{iso}| \leq |\delta_{33} - \delta_{iso}|$. The partial charges of the ring carbons, q(C), and of the cations, $q(M^+)$, were calculated within the GIAO procedure on the same level of theory and with the same basis sets. The chemical shift tensors were extracted from Gaussian 98 outputs using a C program,[33] and subsequently, the POV-ray program[34] was employed to visualize the principal axis system (PAS) within the framework of the clusters.

3. Results and Discussion

3.1. Geometric Data, Mulliken Partial Charges, and Adsorption Energies. We first discuss the geometric data and Mulliken partial charges of the interstitial alkali metal cations in the clusters $\mathbf{T^{M^+}}$, **Z**, and **ZT**. The distances between the cations and the toluene ring plane, d_1, and between the cation and the plane of the sodalite six-ring window (i.e., the zeolite fragment), d_2, as depicted in Figure 3a, are given in Table 1 and also plotted in Figure 4. We define distance to the "plane" as the distance of the cation to the line connecting i-**C** and p-**C** in case of d_1, and the distance of the cation to the line connecting

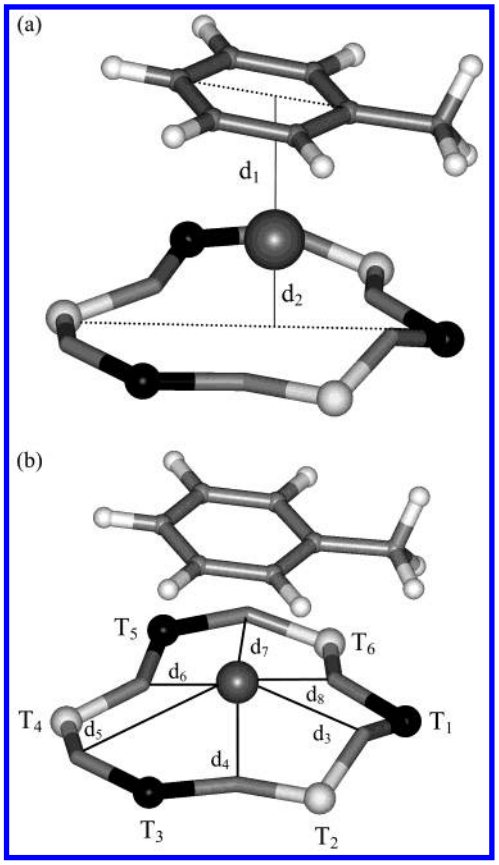

Figure 3. Definition of (a) the distances between cation and toluene ring plane, d_1, and distances between cation and sodalite six-ring window, d_2 and (b) distances between the cation and the six-ring oxygen atoms, d_3−d_8, with the Al atoms in the following positions: $\mathbf{Z^I/ZT^I}$, Al = T_1; $\mathbf{Z^{IIm}/ZT^{IIm}}$, Al = T_1 and T_5; $\mathbf{Z^{IIp}/ZT^{IIp}}$, Al = T_1 and T_4; $\mathbf{Z^{III}/ZT^{III}}$, Al = T_1, T_3, and T_5.

T_1 and T_4 in case of d_2. These definitions were found to give the most consistent sets of data and are adhered to throughout this work. However, it should be borne in mind that both the toluene and zeolite rings distort from their ideal symmetry during optimization. Also tabulated are the distances between the cations and the oxygen atoms of the zeolite fragment (d_3−d_8, as defined in Figure 3b), and finally, the Mulliken partial charges of the cations, $q(M^+)$, are given in Table 1.

Particularly with the **ZT** clusters, a complex set of interactions exists between the zeolite, the cation, and the toluene. The cations act simultaneously as Lewis acids (electron-pair acceptors) both toward the framework oxygen atoms and toward the π-electrons of the aromatic toluene ring. The cation−framework oxygen interaction is, aside from the Al content, decisive in determining the basicity of the zeolite: when the cation is less electronegative, the negative charge of the framework oxygen atoms (i.e., the basicity of the zeolite) is higher.[35] The cation−π-electron interaction mainly governs the position of the toluene above the six-ring window in the zeolite. However, these interactions cannot easily be separated because they appear simultaneously in the real zeolite. Therefore, we first consider two "simple" interactions independently: the toluene−cation interaction in the $\mathbf{T^{M^+}}$ clusters and the cation−zeolite fragment interactions occurring in clusters **Z**. Finally, a comparison of these results with those from the **ZT** clusters, comprising toluene, cation, and zeolite fragment, will enable a fuller discussion of the overall chemistry of the systems.

To investigate the "pure" cation−π-electron interaction established between the cation and the aromatic toluene ring,

TABLE 1: Distances d_1 (Cation−Toluene Ring Plane), d_2 (Cation−Sodalite Six-Ring), and d_3−d_8 (Cation−O-atoms) as Described in Figure 3a,b and Cation Mulliken Partial Charges of the Cations, $q(M^+)$, in Clusters T^{M^+}, ZT^{I}, ZT^{IIm}, ZT^{IIp}, and ZT^{III}

cluster	d_1 (Å)	d_2 (Å)	d_3 (Å)	d_4 (Å)	d_5 (Å)	d_6 (Å)	d_7 (Å)	d_8 (Å)	$q(M^+)$ (au)
T^{Li+}	1.856								0.406
T^{Na+}	2.395								0.722
T^{K+}	2.937								0.935
T^{Rb+}	3.150								0.987
T^{Cs+}	3.390								0.993
$Z^{I} + Li^+$		0.709	1.942	3.386	2.799	3.212	2.072	2.086	1.022
$Z^{I} + Na^+$		1.093	2.251	3.228	2.575	2.998	2.344	2.584	0.983
$Z^{I} + K^+$		1.833	2.635	3.434	2.933	3.227	2.754	2.892	1.000
$Z^{I} + Rb^+$		2.087	2.782	3.524	3.101	3.377	2.929	3.016	0.998
$Z^{I} + Cs^+$		2.510	2.981	3.847	3.570	3.791	3.210	3.094	0.978
$Z^{IIp} + Li^+$		0.361	2.139	2.126	3.206	2.415	3.471	1.898	1.009
$Z^{IIp} + Na^+$		0.964	2.446	2.397	3.111	2.477	3.468	2.215	0.969
$Z^{IIp} + K^+$		1.753	2.770	2.882	3.434	2.905	3.680	2.603	0.991
$Z^{IIp} + Rb^+$		2.078	2.877	3.097	3.664	3.184	3.870	2.754	0.961
$Z^{IIp} + Cs^+$		2.410	3.045	3.378	3.981	3.492	4.029	2.942	0.958
$Z^{IIm} + Li^+$		0.643	1.959	3.605	2.491	3.367	2.057	2.046	1.012
$Z^{IIm} + Na^+$		1.207	2.260	3.628	2.536	3.257	2.319	2.401	0.973
$Z^{IIm} + K^+$		1.980	2.660	3.908	3.017	3.541	2.746	2.728	0.991
$Z^{IIm} + Rb^+$		2.219	2.808	3.986	3.197	3.656	2.903	2.859	0.964
$Z^{IIm} + Cs^+$		2.562	3.023	4.165	3.490	3.922	3.160	3.009	0.959
$Z^{III} + Li^+$		0.220	2.779	1.953	3.434	2.160	3.208	1.881	0.996
$Z^{III} + Na^+$		1.208	2.447	2.334	3.710	2.522	3.426	2.209	0.959
$Z^{III} + K^+$		2.147	2.709	2.965	4.262	3.210	3.837	2.606	0.982
$Z^{III} + Rb^+$		2.552	2.886	3.157	4.603	3.785	4.058	2.775	0.958
$Z^{III} + Cs^+$		2.899	3.017	3.438	4.907	4.158	4.352	3.043	0.951
$ZT^{I} + Li^+$	2.814	0.962	1.993	3.418	2.902	3.290	2.176	2.077	1.048
$ZT^{I} + Na^+$	2.614	1.195	2.284	3.248	2.624	3.034	2.391	2.596	0.980
$ZT^{I} + K^+$	2.839	1.709	2.611	3.370	2.796	3.111	2.688	2.918	1.072
$ZT^{I} + Rb^+$	3.179	2.069	2.798	3.460	3.007	3.325	2.960	3.103	1.035
$ZT^{I} + Cs^+$	3.287	2.308	2.912	3.581	3.191	3.532	3.163	3.251	1.045
$ZT^{IIp} + Li^+$	2.813	0.664	2.073	2.247	3.308	2.567	3.512	1.940	1.005
$ZT^{IIp} + Na^+$	2.645	1.077	2.457	2.460	3.160	2.537	3.490	2.250	0.939
$ZT^{IIp} + K^+$	2.876	1.689	2.743	2.797	3.356	2.864	3.695	2.605	1.025
$ZT^{IIp} + Rb^+$	3.077	1.978	2.853	2.969	3.520	3.090	3.872	2.756	0.990
$ZT^{IIp} + Cs^+$	3.310	2.296	3.003	3.203	3.785	3.378	4.044	2.952	1.012
$ZT^{IIm} + Li^+$	2.882	0.881	1.999	3.648	2.595	3.431	2.131	2.021	1.022
$ZT^{IIm} + Na^+$	2.665	1.360	2.315	3.691	2.645	3.325	2.377	2.398	0.957
$ZT^{IIm} + K^+$	2.893	1.925	2.665	3.898	2.950	3.462	2.687	2.734	1.033
$ZT^{IIm} + Rb^+$	3.085	2.170	2.820	3.994	3.140	3.571	2.829	2.851	0.961
$ZT^{IIm} + Cs^+$	3.269	2.513	3.146	4.207	3.325	3.657	3.019	3.102	1.002
$ZT^{III} + Li^+$	3.363	0.392	2.728	1.959	3.449	2.207	3.227	1.887	1.031
$ZT^{III} + Na^+$	2.771	1.380	2.444	2.441	3.815	2.640	3.474	2.253	0.927
$ZT^{III} + K^+$	2.853	1.945	2.772	2.808	4.008	2.925	3.698	2.567	0.974
$ZT^{III} + Rb^+$	3.045	2.357	3.028	2.950	4.194	3.367	3.871	2.753	0.903
$ZT^{III} + Cs^+$	3.318	2.694	3.166	3.228	4.468	3.685	4.080	2.961	0.963

we present results of calculations on the toluene−cation clusters. Because the interaction with the π-electrons[36] is the most favorable, the cation is localized above the aromatic ring plane. The cation acts as Lewis acid and, hence, is expected to polarize the electron cloud of the aromatic ring. Of all of the alkali metals, Li^+ has the strongest cation−aromatic ring interaction because lithium is the most electronegative of this group. As can be seen from the d_1 values in Table 1 and Figure 4, Li^+ is closest to the aromatic ring plane and its Mulliken partial charge is reduced substantially to 0.406 au, while the bigger and less electronegative Cs^+ is the most distant and its charge is only decreased to 0.993 au. For all **Z** clusters, Li^+ is closest to the plane of the zeolite six-ring fragment and Cs^+ is the most distant. Cs^+ is about 2 Å more distant than Li^+ from the sodalite ring plane for clusters $\mathbf{Z^{I}}$, $\mathbf{Z^{IIm}}$, and $\mathbf{Z^{IIp}}$ but almost 3 Å more distant in cluster $\mathbf{Z^{III}}$. The Li^+ cation has the most-positive Mulliken partial charge, whereas Cs^+ shows less-positive values. In general, when going from lower to higher aluminum content the cation charges decrease because of the higher basicity of the adjacent framework oxygen atoms.

The distances d_1 and d_2 are presented graphically for clusters **ZT** and $\mathbf{T^{M^+}}$ in Figure 4. Among all of the **ZT** clusters, Na^+ has the shortest distance to the toluene ring plane. The order of cations according to increasing d_1 in these clusters is $Na^+ < Li^+ < K^+ < Rb^+ < Cs^+$ ($\approx Li^+$ in cluster $\mathbf{ZT^{III}}$). The difference in d_1 between Li^+ and Na^+ is about 0.2 Å for clusters $\mathbf{ZT^{I}}$, $\mathbf{ZT^{IIm}}$, and $\mathbf{ZT^{IIp}}$ but 0.6 Å for $\mathbf{ZT^{III}}$. Cs^+ is about 0.5−0.7 Å more distant from the aromatic ring plane than Na^+. Li^+ is very strongly embedded in the zeolite six-ring of $\mathbf{ZT^{III}}$ ($d_2 = 0.39$ Å) and most distant in the case of $\mathbf{ZT^{I}}$ ($d_2 = 0.96$ Å), while for Cs^+, d_2 can be up to 2.69 Å in the case of cluster $\mathbf{ZT^{III}}$. A comparison with clusters **Z** shows that Li^+ and Na^+ are up to 0.3 Å closer to the plane of the zeolite fragment when the additional interaction with the aromatic toluene ring is absent. Conversely, K^+, Rb^+, and Cs^+ are found from 0.05 Å up to 0.20 Å closer to the plane of the fragment when toluene is

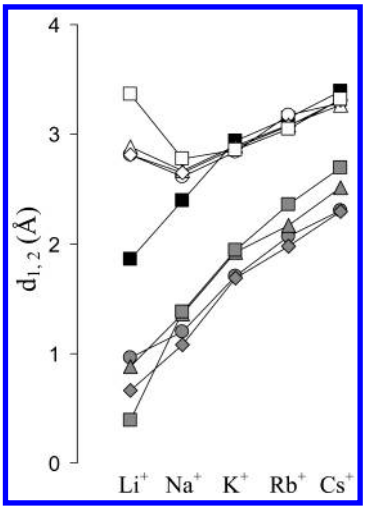

Figure 4. Distances between cation and toluene ring plane (d_1, open symbols) and distances between cation and sodalite six-ring window (d_2, shaded symbols) for clusters $\mathbf{T^{M^+}}$ (■), $\mathbf{ZT^{I}}$ (○), $\mathbf{ZT^{IIm}}$ (△), $\mathbf{ZT^{IIp}}$ (◇), and $\mathbf{ZT^{III}}$ (□), respectively.

present. The Mulliken partial charges are smaller in value for Na^+ and Rb^+ than they are for the other interstitial cations. Only with $\mathbf{T^{M^+}}$ clusters do the Mulliken partial charges of the cations correlate strongly with the distances d_1, as would be expected (linear correlation coefficient $r = 0.97$). However, in clusters **Z** and **ZT**, no simple correlations can be obtained because of the complex intermolecular interactions that exist.

The oxygen cation distances d_3-d_8, defined in Figure 3b, show the positions of the cations with respect to the oxygen atoms in the six-membered ring of the zeolite fragment. The cations are displaced toward those oxygen atoms that are bonded to aluminum atoms, with Li^+ being closest and Cs^+ the most distant.[36] Because the tetravalent framework position is occupied by trivalent Al, there is an excess of electron density in that part of the ring fragment, which explains the observed shifts toward its adjacent oxygen atoms. In clusters **TZ**, the cation is more distant from the ring oxygen atoms than in clusters **Z**. In addition to the plane distances, we also studied the distances between all seven toluene carbon atoms and the corresponding cations, $d(C-M^+)$, which are compiled in Table 2 for the clusters $\mathbf{T^{M^+}}$, $\mathbf{ZT^{I}}$, $\mathbf{ZT^{IIm}}$, $\mathbf{ZT^{IIp}}$, and $\mathbf{ZT^{III}}$, together with the Mulliken partial charges of the different toluene carbon atoms, q(C).

In Figure 5a−d, the distances $d(C-M^+)$ and partial charges q(C) data for the different clusters under consideration are graphed. Figure 5a,c plots the sequences for each cluster separately with respect to decreasing electronegativity of the interstitial cations, while Figure 5b,d shows the influence of increasing Al amount in the fragment on these values. In Figure 5a, inspection of $d(C-M^+)$ reveals for $\mathbf{T^{M^+}}$ a continuous increase of $d(C-M^+)$ from Li^+ to Cs^+, whereas for the **ZT** clusters, this quantity decreases from Li^+ to Na^+ and increases again from Na^+ to Cs^+ (comparable to the trends presented in Figure 4). For o-C′ and m-C′ of Li^+ clusters $\mathbf{ZT^{I}}$ and $\mathbf{ZT^{IIm}}$, a continuous decrease is observed in distances from Li^+ to Cs^+. The i-**C** and both of the o-**C** are always closest to the cation, that is, the cation is not exactly located above the middle but shifted toward the $\mathbf{C}H_3$ group of the molecule. Compared to $\mathbf{T^{M^+}}$, the methyl carbons are closer (up to 0.6 Å) to the cation for Na^+, K^+, Rb^+, and Cs^+ **ZT** clusters, but in the case of Li^+ **ZT** clusters, they are more distant (up to 0.4 Å). However, all of the ring carbon atoms are more distant in the case of Li^+ and Na^+ (from 0.1 to 2.2 Å and less for Na^+ than for Li^+), whereas the distances $d(\mathbf{C}_{ar}-K^+)$, $d(\mathbf{C}_{ar}-Rb^+)$, and $d(\mathbf{C}_{ar}-Cs^+)$ are only up to 0.3 Å different from the corresponding distances in the clusters $\mathbf{T^{M^+}}$.

The aromatic ring of toluene is not always parallel to the plane of the sodalite cage six-membered ring fragment in clusters **ZT**, as can easily be seen from the distances between the Li^+ cation and the two o-**C**'s (○) and two m-**C**'s (▽) illustrated in Figure 5b. These values are clearly distinguished, that is, on one side of the ring o-**C**′ and m-**C**′ are closer to the cation than their counterparts o-**C**″ and m-**C**″ on the opposite side of the ring. The differences between the distances d(o-**C**′$-M^+$) and d(o-**C**″$-M^+$) and d(m-**C**′$-M^+$) and d(m-**C**″$-M^+$), respectively, became smaller from Li^+ to Cs^+. Δd(o-**C**′$-Li^+$) and Δd(o-**C**′$-Li^+$) are 0.9, 0.2, 0.7, and 0.2 Å for clusters $\mathbf{ZT^{I}}$, $\mathbf{ZT^{IIp}}$, $\mathbf{ZT^{IIm}}$, and $\mathbf{ZT^{III}}$, respectively. The tilting of toluene along its i-**C**−p-**C** axis is responsible for the different trend, mentioned above, found with Li^+ clusters $\mathbf{ZT^{I}}$ and $\mathbf{ZT^{IIm}}$.

In Figure 5c, the Mulliken partial charges, q(C), are presented for each cluster as a function of alkali cation. The most significant changes in the partial charges appear with the i-**C** and both of the o-**C** carbon atoms. These are the atoms that are closest to the cations. Clear trends can be seen only with cluster $\mathbf{T^{M^+}}$ in which again the atoms i-**C** and both of the o-**C** show the most significant changes with Δq(C) of about 0.6 au when going from Li^+ to Cs^+. When plotted for each cation in terms of cluster composition (Figure 5d), fewer trends are observed. Indeed for the Li^+ and Na^+ **ZT** clusters, with their closer proximity of zeolite and molecule, there is considerable variation of the q(C) values with Al content. However, in general, it can be seen that the negative charge of the carbons increases in the series $\mathbf{C}H_3$ > m-**C** > o-**C** ≈ p-**C** > i-**C**.

The adsorption energies, E_{ads}, of toluene adsorbed on a specific cluster **TZ** have been calculated as the difference between the total energy of that cluster **TZ** and the sum of the total energies of the corresponding cluster **Z** and the total energy of toluene, that is, $E_{ads} = E_{\mathbf{TZ}} - (E_{\mathbf{Z}} + E_{\mathbf{T}})$. In Figure 6, the adsorption energies are plotted versus decreasing cation electronegativity. For all **TZ** clusters, toluene is most strongly adsorbed on Na^+ clusters. E_{ads} is mainly governed by the cation$-\pi$-electron interaction, so the electronegativity of the cation is the decisive factor in determining the strength of adsorption. Li^+, the cation with the highest electronegativity, is so close to the zeolite fragment that it is sterically prevented from interacting fully with the aromatic ring. However Na^+, the second most electronegative, is sufficiently exposed to interact with the toluene most strongly. The other cations are also accessible to the toluene molecule, but they interact more weakly as their electronegativity decreases. The adsorption energies correlate reasonably well with the distances between cation and toluene ring plane, d_1($r = 0.93$, 0.99, 0.92, and 0.92 for $\mathbf{TZ^{I}}$, $\mathbf{TZ^{IIm}}$, $\mathbf{TZ^{IIp}}$, and $\mathbf{TZ^{III}}$, respectively).

3.2. NMR Data. The magnitude of the chemical shift, depending on the local symmetry at the nuclear site, will vary as a function of the orientation of the molecule with respect to the external magnetic field. This orientation dependence is referred to as chemical shift anisotropy (CSA). The relevant values constitute the symmetric part of the full chemical shift tensor, which consists of six independent components. The chemical shift tensor can be expressed in a coordinate system in which all off-diagonal elements vanish. Hence, CSA is fully described by the three diagonal elements δ_{11}, δ_{22}, and δ_{33} (the principal components). The associated eigenvectors (referred to as the principal axis system, PAS) give the orientation of the tensor relative to the molecular frame system. In Figure 7,

TABLE 2: Distances between the Seven Toluene Carbon Atoms and the Cations, $d(C-M^+)$, and Mulliken Partial Charges of the Toluene Carbon Atoms, $q(C)$, for Clusters T, T^{M^+}, ZT^{I}, ZT^{IIm}, ZT^{IIp}, and ZT^{III}

	T		**T^{M+}**		**ZT^{I}**		**ZT^{IIp}**		**ZT^{IIm}**		**ZT^{III}**	
	q(C) [au]		d(C−M^+) [Å]	q(C) [au]	d(C−M^+) [Å]	q(C) [au]	d(C−M^+) [Å]	q(C) [au]	d(C−M^+) [Å]	q(C) [au]	d(C−M^+) [Å]	q(C) [au]
CH_3	−0.549	Li^+	3.528	−0.639	3.666	−0.758	3.888	−0.879	3.949	−0.700	3.684	−0.529
		Na^+	3.909	−0.635	3.722	−0.759	3.863	−0.869	3.826	−0.556	3.579	−0.612
		K^+	4.288	−0.600	3.881	−0.589	3.854	−0.677	3.915	−0.677	3.799	−0.537
		Rb^+	4.441	−0.513	4.047	−0.572	3.890	−0.565	3.985	−0.593	3.908	−0.576
		Cs^+	4.626	−0.479	4.066	−0.576	4.030	−0.580	4.120	−0.532	4.127	−0.581
C−CH_3	1.328	Li^+	2.358	0.036	2.922	0.741	3.033	−0.015	3.106	1.036	3.363	0.054
		Na^+	2.827	0.024	2.849	0.505	2.942	−0.097	2.934	0.391	2.853	0.578
		K^+	3.306	0.191	3.057	0.600	3.076	0.226	3.133	0.226	3.044	0.371
		Rb^+	3.499	0.557	3.341	0.405	3.224	0.272	3.266	0.438	3.217	0.389
		Cs^+	3.721	0.624	3.423	0.360	3.414	0.396	3.430	0.576	3.468	0.435
o-**C**	−0.853	Li^+	2.318	0.257	2.562	−0.991	2.936	0.738	2.780	−0.938	3.569	0.014
					3.470	0.278	3.202	0.346	3.462	−0.028	3.766	−0.693
		Na^+	2.781	0.179	2.848	−0.278	2.885	0.735	2.938	−0.282	3.060	0.103
					2.964	0.108	3.014	0.253	2.990	0.071	2.965	−0.317
		K^+	3.263	−0.032	3.120	−0.342	3.132	0.104	3.163	−0.110	3.147	0.065
					3.133	−0.136	3.150	−0.110	3.195	0.104	3.104	−0.278
		Rb^+	3.456	−0.312	3.398	−0.294	3.323	−0.007	3.344	−0.321	3.295	−0.105
					3.434	0.001	3.323	−0.176	3.328	0.005	3.303	−0.119
		Cs^+	3.679	−0.357	3.483	−0.306	3.539	−0.084	3.526	−0.333	3.542	−0.113
					3.553	−0.023	3.519	−0.320	3.485	−0.137	3.549	−0.336
m-**C**	0.120	Li^+	2.311	−0.471	2.894	−0.139	3.066	−0.709	2.915	0.122	4.160	−0.179
					3.723	−0.036	3.343	−0.652	3.574	−0.183	4.330	0.276
		Na^+	2.745	−0.469	2.990	−0.260	2.950	−0.669	3.036	−0.331	3.387	−0.553
					3.106	−0.407	3.091	−0.559	3.083	−0.699	3.310	−0.614
		K^+	3.229	−0.382	3.228	−0.333	3.287	−0.384	3.265	−0.442	3.303	−0.475
					3.243	−0.377	3.290	−0.442	3.292	−0.384	3.271	−0.553
		Rb^+	3.424	−0.309	3.560	−0.345	3.515	−0.357	3.489	−0.321	3.457	−0.411
					3.590	−0.330	3.511	−0.457	3.474	−0.490	3.464	−0.451
		Cs^+	3.643	−0.302	3.668	−0.333	3.756	−0.296	3.678	−0.370	3.706	−0.338
					3.735	−0.320	3.746	−0.376	3.636	−0.470	3.711	−0.362
p-**C**	−0.515	Li^+	2.319	−0.159	3.479	−0.475	3.285	−0.193	3.337	−0.834	4.519	−0.431
		Na^+	2.743	−0.221	3.119	−0.275	3.064	−0.189	3.111	0.058	3.514	−0.026
		K^+	3.220	−0.285	3.285	−0.261	3.363	−0.185	3.322	−0.185	3.361	−0.081
		Rb^+	3.411	−0.354	3.652	−0.250	3.600	−0.168	3.552	−0.110	3.536	−0.138
		Cs^+	3.629	−0.355	3.783	−0.226	3.866	−0.216	3.730	−0.169	3.788	−0.189

the orientation of the ^{13}C chemical shift tensors within toluene alone is presented. For the aromatic carbons, the most-shielded component, δ_{33}, is perpendicular to the ring plane. δ_{11}, the least-shielded component, lies in the aromatic ring plane pointing toward its center, and δ_{22} is found in the ring plane, orientated orthogonally to δ_{11} and δ_{33}. For the methyl carbon, δ_{33} is coincident with the C−CH_3 bond, while δ_{22} lies in the ring plane, and δ_{11} is orthogonal to the ring plane. In the clusters $\mathbf{T^{M^+}}$ and **ZT**, the components are slightly tilted from the positions that they have in isolated toluene because of interactions with the cation and the zeolite fragment. In Figures 8, 9, and 10, respectively, the ^{13}C chemical shift data, that is, δ_{iso}, δ_{11}, δ_{22}, δ_{33}, δ_{aniso}, and η, are presented for the 26 different clusters under consideration. In Figures 8−10, the upper plots display the ^{13}C NMR data for each cluster as they vary with decreasing electronegativity of the interstitial alkali metal cation, whereas the lower graphs display the data for all clusters with the same cation but as a function of different/increasing Al content. Again, the same data is plotted twice, enabling us to visualize separately the dependence of the NMR parameters on the identity of the cation and on increasing Al/Si ratio. In all of the graphs, the corresponding values calculated for the isolated toluene are also included to provide a comparison with the interaction-free molecule. In Figure 8a,b, the isotropic chemical shift data, δ_{iso}, are presented. In general, the carbon chemical shifts increase in the order **C**H_3 < p-**C** < m-**C** ≤ o-**C** < **C**−CH_3 (i.e., methyl carbon is the most-shielded). These data do not show significant trends with respect either to the identity of the cation or to the framework composition. However, the isotropic shift data for the Li^+-containing clusters show considerable scatter. The strong tilt of the molecule (up to 0.9 Å) causes a difference in chemical environment for the single toluene carbon atoms and therefore shifts can vary up to 10 ppm. This is most apparent for the o-**C′** carbon atom of the Li^+ cluster $\mathbf{ZT^{I}}$ (see Figure 8a). In addition, the proximity of the framework and sorbate molecule for the Li-zeolites will result in a more complex series of interactions than those for the larger cations, and it is also therefore likely that these Li^+ results are more-dependent on the zeolite model employed, that is, the size of the cluster and its method of termination.

However, the case is different with the individual tensor components, δ_{11}, δ_{22}, and δ_{33}, many of which show considerable variation. The relation between the isotropic chemical shift and the components is $|\delta_{iso} - \delta_{33}| \geq |\delta_{iso} - \delta_{11}| \geq |\delta_{iso} - \delta_{22}|$ and $\delta_{11} \geq \delta_{22} \geq \delta_{iso} \geq \delta_{33}$. In Figure 8c,d, the data of the least-shielded component, δ_{11}, are presented. As the electronegativity of the interstitial cation decreases, the aromatic carbons are generally more-deshielded (i.e., they have higher chemical shift values). The clearest trends can be seen with the simple cluster $\mathbf{T^{M^+}}$ because only the cation−aromatic ring interaction has to be considered. However, in varying degrees, all of the **ZT** clusters also show this trend to lower field for the ring carbon atoms. The data for methyl carbon show hardly any variation. In Figure 8d, which shows the variation of component δ_{11} with

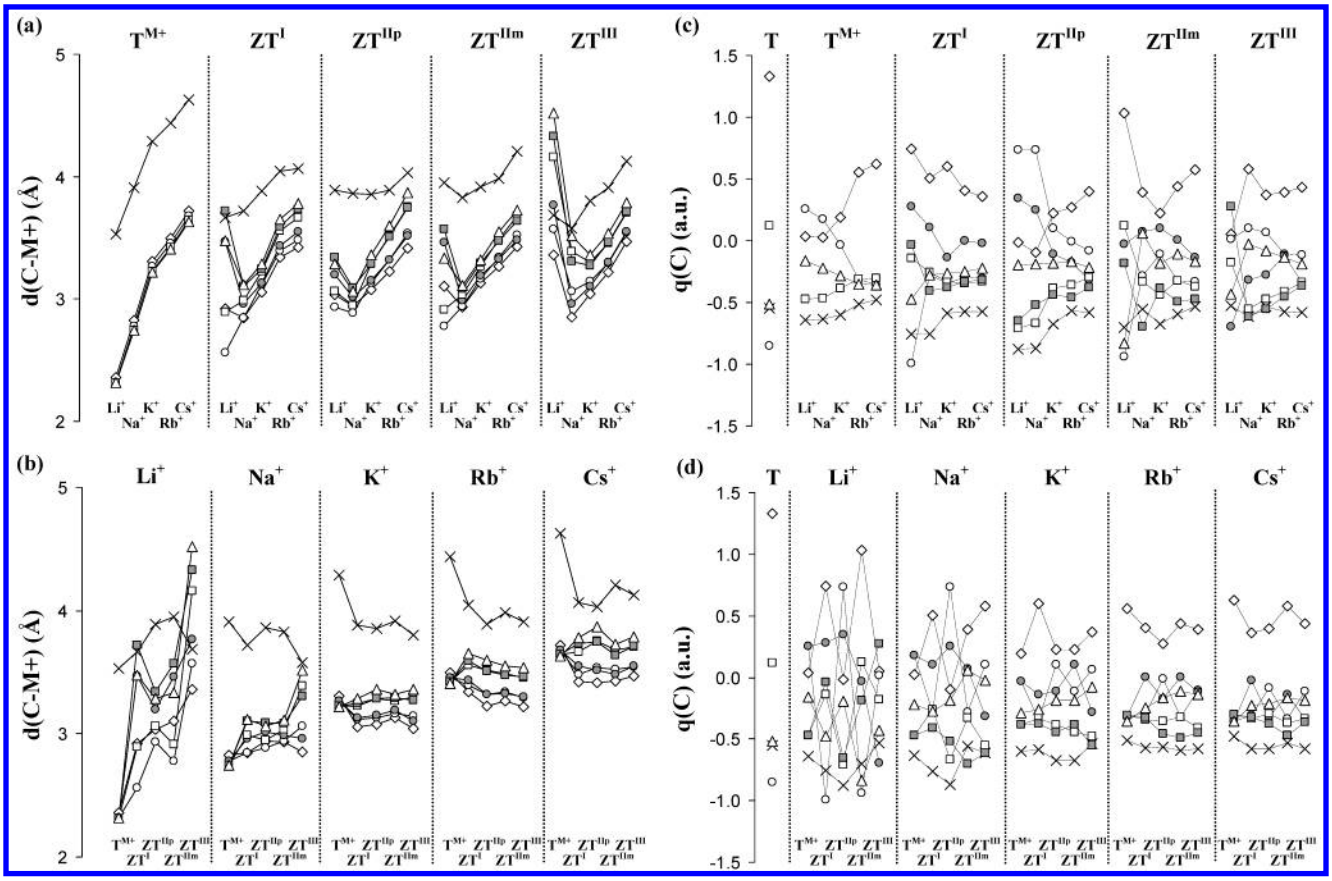

Figure 5. Plot displaying distances between the toluene carbons and the interstitial alkali metal cations, $d(C-M^+)$, and the Mulliken partial charges of the toluene carbons, $q(C)$, for (a, c) each cluster with respect to the decreasing electronegativity for the cations and (b, d) for each cation with respect to increasing Al amount. The carbons are indicated as follows: **C**H_3 (×), **C**$-CH_3$ (◇), o-**C** (○), m-**C** (□), and p-**C** (△) (open symbols and shaded symbols indicate adjacent o- and m-**C**, respectively).

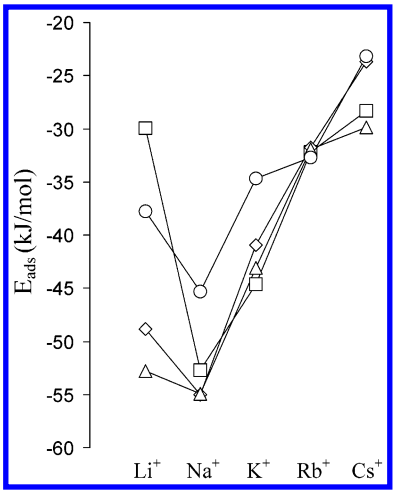

Figure 6. Adsorption energies, E_{ads}, of toluene adsorbed at the six-ring window/S_{II} site: **ZT^{I}** (○), **ZT^{IIm}** (△), **ZT^{IIp}** (◇), and **ZT^{III}** (□).

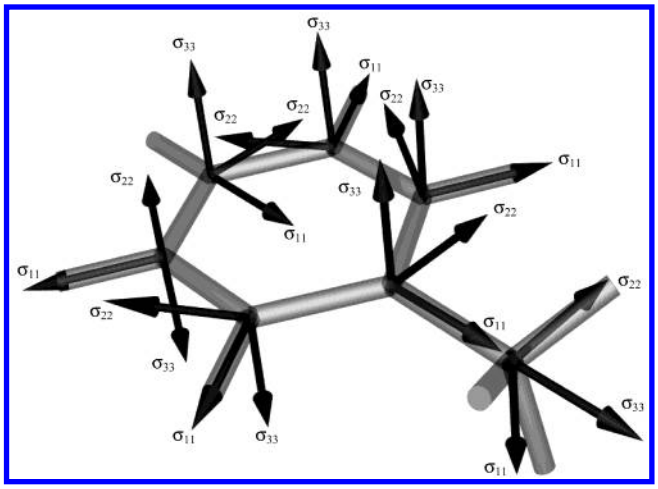

Figure 7. Orientations of the principal components δ_{11}, δ_{22}, and δ_{33} of the ^{13}C shift tensors displayed within the framework of the toluene molecule.

respect to aluminum content, the data for the Li^+-containing **ZT** clusters again show considerable scatter, due to the reasons given before. Figure 9 contains plots of δ_{22} and δ_{33}. In Figure 9a, the δ_{22} values for the all of the carbon atoms do not vary greatly, except those of the i-**C** carbons, which change significantly over a range of 20 ppm. For clusters **T^{M+}**, all of the δ_{22} values of the aromatic carbons are shifted toward higher field when the electronegativity of the interstitial cation decreases. Again, the Li^+ data are most sensitive toward changes in the Si/Al environment. The **C**H_3 carbons are hardly affected by changing the Al amount in the zeolite fragments and, hence, do not show significant changes. In Figure 9c,d, plots of the most-shielded tensor component, δ_{33}, are presented. For both o-**C**′ and o-**C**″, δ_{33} is the most-deshielded component. The sequence of carbon atoms according to increasing shielding (i.e., lower shift values) is o-**C** > m-**C** ≥ i-**C** > p-**C** > **C**H_3, as can be readily seen in Figure 9c. For all clusters and cations, the shifts of o-**C**′ and o-**C**″ are clearly separated (up to 5 ppm). The parameter δ_{33} of the methyl carbons is the most-shielded and becomes more-shielded (total range ∼10 ppm) with decreasing electronegativity of the interstitial cation. In other words, the electron density along component δ_{33} increases for

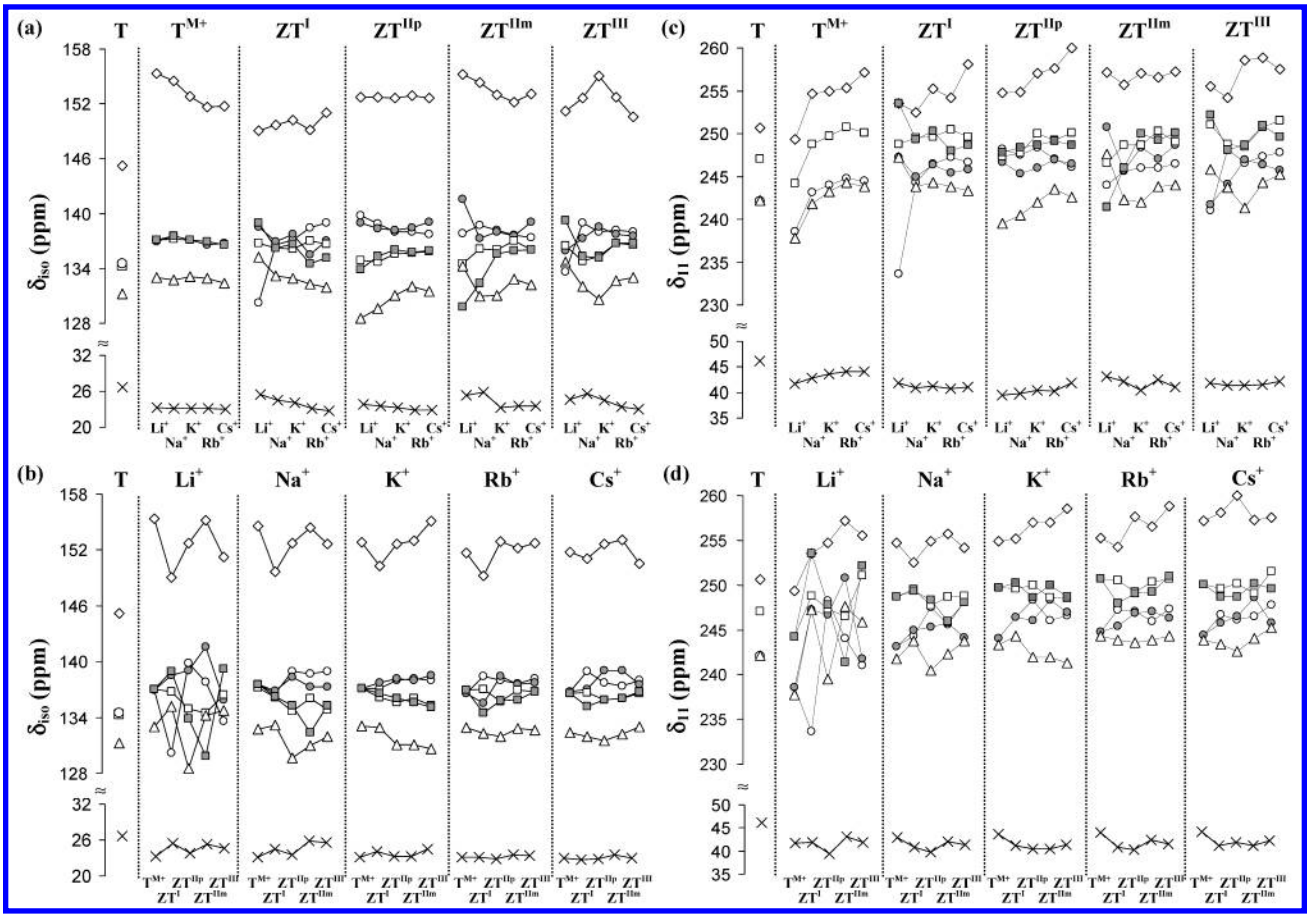

Figure 8. Plot displaying the isotropic chemical shifts, δ_{iso}, and the less-shielded principal components, δ_{11}, for (a, c) each cluster with respect to decreasing electronegativity of the cations and (b, d) each cation with respect to increasing Al amount. The carbons are indicated as follows: **C**H_3 (×), **C**−CH_3 (◇), o-**C** (○), m-**C** (□), and p-**C** (△) (white symbols and gray symbols indicate adjacent o- and m-**C**).

the **C**H_3 carbon atoms, and they are negatively polarized along the i-**C**−**C**H_3 bond. This result accords with commonly accepted theory first expounded by Itoh et al.[14] of the negative polarization of the **C**H_3 carbon, which facilitates the attack of the reactive alkylating species. The fact that the isotropic chemical shift barely changes for **C**H_3 carbons also accords with Hunger et al.,[2] who could not find any evidence of polarization of the methyl group by studying isotropic shifts. In terms of defining descriptors that could offer discrimination between sites of different composition, the isotropic shifts only of the i-**C** and the two o-**C** atoms seem to be suitable. For the **C**H_3 carbons, the individual tensor components are revealing, and thus an NMR method from which the anisotropic shift parameters may be extracted should be employed.

Overall, it is clear that the two different factors that we have chosen to study (i.e., the trends due to the nature of the alkali cation and due to increasing amount of Al atoms in the fragment) give different pictures. When considering how the NMR parameters depend on the increasing size and electropositivity of the interstitial cation, we observe plots with smooth curves and recognizable trends. In other words, the electron distribution in the toluene molecule is influenced directly by the interaction with the cations, with the Lewis acidities of the cations tuned by interaction with a zeolite fragment of given composition. But when examining the influence of varying framework composition with the same cation, the complex nature of the chemical interactions, both within the zeolite fragment and in the way the zeolite affects the cation−molecule interaction, becomes apparent. The result is plots with no clear-cut trends. Therefore, it is not possible to obtain a straightforward relation between NMR parameters and chemical environment, as would be expected in simple systems. Here, we only observe the net result of a range of interactions in terms of perturbing the Lewis acidity of a cation, which is the most important factor in determining chemical shift parameters.

Finally, we will present two further quantities: the anisotropy parameter, δ_{aniso}, and the asymmetry parameter, η (see Figure 10a−d). The anisotropy parameters, δ_{aniso}, express the magnitude of anisotropy of a nucleus (i.e., the range of nuclear orientations with regards to the external magnetic field $\mathbf{B}_0$), and they are plotted in Figure 10a,b for clusters **T**, $\mathbf{T^{M+}}$, and **ZT**. The **C**H_3 carbons have the smallest δ_{aniso}, while the i-**C** carbons have the largest values. The sequence of carbon atoms with increasing anisotropy parameter is as follows: i-**C** > p-**C** = m-**C** > o-**C** > **C**H_3. With decreasing electronegativity of the interstitial cation, no significant changes in the δ_{aniso} of the **C**H_3 carbons are recognizable. Again, plotting the parameters according to cation (Figure 10a) results in clearer trends than doing so in with respect to framework composition (Figure 10b).

The asymmetry parameters, η, which are plotted in Figure 10c,d, give information about the neighborhood of a carbon atom under consideration. A value of $\eta = 0$ denotes a highly symmetric environment, while $\eta = 1$ indicates a highly asymmetric environment. The **C**H_3 and i-**C** carbons have the lowest asymmetry parameter because they are situated in the more symmetric moiety of the toluene molecule. All of the other aromatic carbons show values higher than $\eta = 0.55$. For $\mathbf{T^{M+}}$, η increases with decreasing cation electronegativity for all of the carbon atoms under consideration.

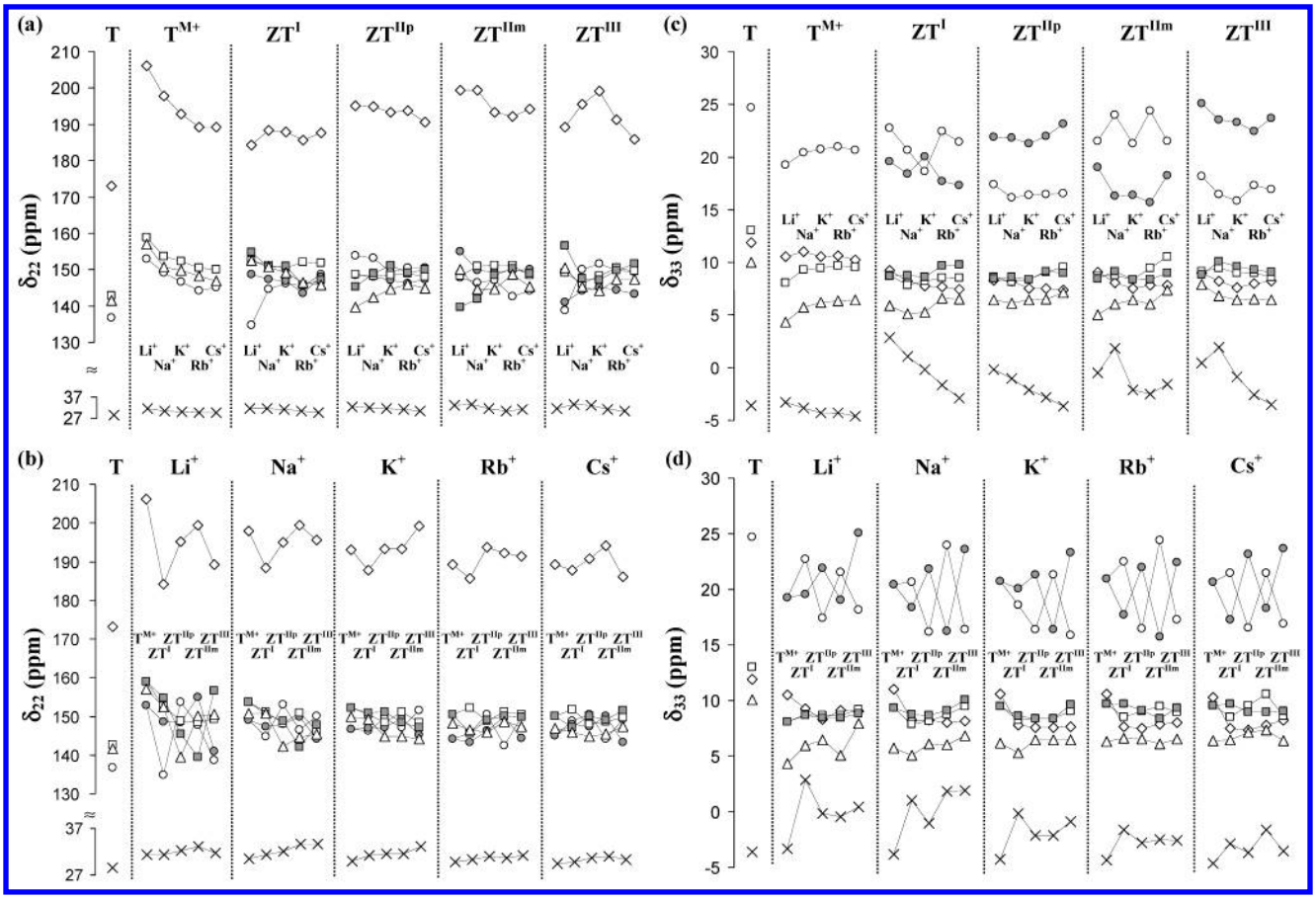

Figure 9. Plot displaying the medium-shielded principal component, δ_{22}, and the most-shielded principal component, δ_{33}, for (a, c) each cluster with respect to decreasing electronegativity of the cations and (b, d) each cation with respect to increasing Al amount. The carbons are indicated as follows: **C**H_3 (×), **C**$-CH_3$ (◇), o-**C** (○), m-**C** (□), and p-**C** (△) (white symbols and gray symbols indicate adjacent o- and m-**C**).

4. Conclusions

Force field calculations and quantum mechanical methods have been employed to model the adsorption of toluene on basic zeolites X and Y with respect to the nature of the cation and the Si/Al ratio. Geometry optimizations and subsequent calculations of partial charges, adsorption energies, and ^{13}C chemical shift parameters of representative cluster models give insight into this adsorption, proposed as the initial step of an important alkylation process catalyzed by basic zeolites. With Monte Carlo docking, we identified the sodalite six-ring window, with SII cation, as a most likely interaction site for the toluene molecule, which is also in accordance with experiment.[19] Cluster calculations revealed more information about the placement of the cations and the toluene molecule with respect to this six-ring window. The cations are shifted toward the oxygen atoms adjacent to the tetrahedral-coordinated Al atoms, and the less electronegative (and larger) the cations are, the more distant they are to the sodalite six-ring window. This latter distance is not influenced by the Si/Al ratio in the zeolite fragment. However, the distance between the aromatic ring plane of toluene and the cation is influenced by the nature of the interstitial cation, which is in turn tuned by the number and location of the Al atoms. Study of the distances between toluene carbon atoms and the cation add further detail to this finding. The sodium cation comes closest to the toluene ring plane, and the toluene is most strongly adsorbed in Na^+ **ZT** clusters. This contrasts with the case of the pure cation−toluene interaction, for which Li^+ has the strongest interaction. In the zeolite however, Li^+ is occluded in the six-ring and as a consequence is less accessible to the aromatic molecule, as described above.

The ^{13}C NMR shift parameters of the aromatic carbons are very sensitive to the concurrent interactions with both interstitial alkali metal cations and the zeolite fragment. The isotropic chemical shifts reveal few significant trends, but the principal components, δ_{11}, δ_{22}, and δ_{33}, show significant trends and changes, as do the anisotropy parameter, δ_{aniso}, and the asymmetry factor, η. The principal components can be represented as vectors within the molecular framework of toluene and will be an appropriate tool to explain and supplement information from NMR experiments. The clearest trends in shift parameters with respect to decreasing electronegativity of the cation, or increasing Al amount, are found with the simple toluene−cation cluster, $\mathbf{T^{M+}}$. In the zeolitic clusters, the toluene encounters cations of which the chemistry is tuned by the nature of the zeolite fragment, and vice versa. When considering shift parameters in terms of the identity of the cation for a given framework composition, on the whole we find continuous trends. In terms only of differing Si/Al ratio, discontinuities are observed, especially with the o-**C**, m-**C**, p-**C,** and always with Li^+, which is deeply embedded in the zeolite six-ring. According to Itoh et al.,[14] drastic changes in shift parameters of the **C**H_3 carbon ought to occur if the molecule is sufficiently polarized to be susceptible to electrophilic attack. When looking simply at the δ_{iso} values, we find hardly any changes either due to different cation electronegativity or due to Al content, in agreement with experimental findings of Hunger et al.[2] Nevertheless, a closer inspection of δ_{33} data of the **C**H_3 carbons reveals a trend to higher field and, therefore, higher electron density in that region. However, substantial polarization of the methyl carbon by one of the basic oxygen atoms of the zeolite

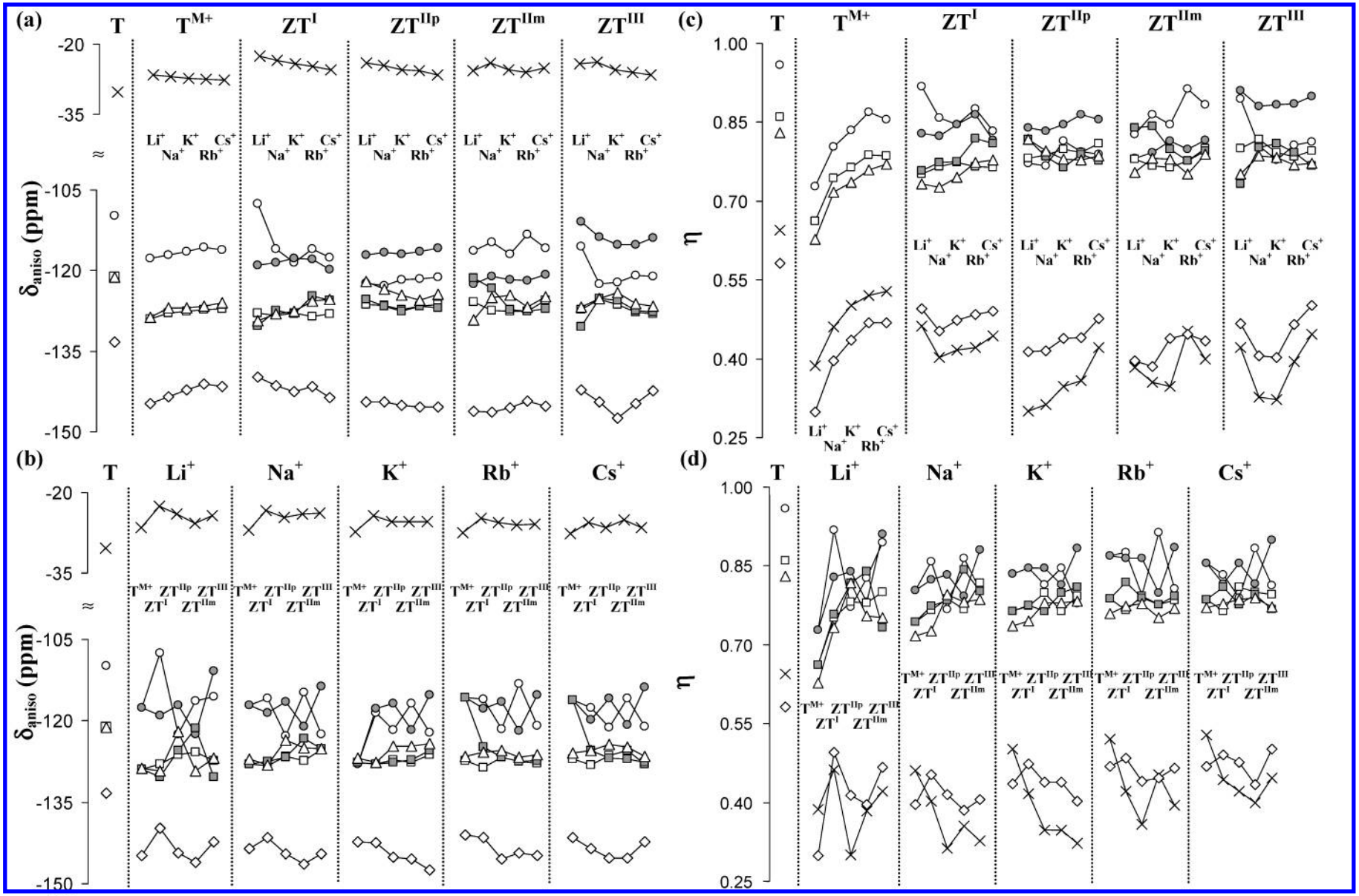

Figure 10. Plot displaying the anisotropy parameter, δ_{aniso}, and the asymmetry factor, η, for (a, c) each cluster with respect to the decreasing electronegativity for the cations and (b, d) each cation with respect to increasing Al amount. The carbons are indicated as follows: **C**H_3 (×), **C**−CH_3 (◇), o-**C** (○), m-**C** (□), and p-**C** (△) (white symbols and gray symbols indicate adjacent o- and m-**C**).

framework is not observed and would appear to be a high-energy process. The indication from our work is that the adsorption process of a single molecule in fully crystalline alkali X or Y zeolite does not itself give rise to the activation of toluene. However detailed consideration of the mechanism of activation is outside the scope of this work and will form the subject of a future study.

Acknowledgment. The authors thank EPSRC and the Leverhulme Trust for financial support, A. A. Sokol (The Royal Institution of Great Britain) for helpful discussion, and D.-P. Luigi, who also wrote and provided programs to extract the relevant NMR data from GAUSSIAN 98 outputs and to visualize the PAS within the clusters.

References and Notes

(1) Hunger, M.; Schenk, U.; Seiler M.; Weitkamp, J. *J. Mol. Catal. A* **2000**, *156*, 153.
(2) Hunger, M.; Schenk, U.; Weitkamp, J. *J. Mol. Catal. A* **1998**, *134*, 97.
(3) Palomares, A. E.; Eder-Mirth, G.; Rep, M.; Lercher, J. A. *J. Catal.* **1998**, *180*, 56.
(4) Wieland, W. S.; Davies, R. J., Garces, J. M. *J. Catal.* **1998**, *173*, 490.
(5) Das, N. K.; Pramanik, K. *J. Indian Chem. Soc.* **1997**, *74*, 701.
(6) Palomares, A. E.; Eder-Mirth, G., Lercher, J. A. *J. Catal.* **1997**, *168*, 442.
(7) Mirth, G.; Lercher, J. A. *J. Catal.* **1994**, *147*, 199.
(8) Philippou, A.; Anderson, M. W. *J. Am. Chem. Soc.* **1994**, *116*, 5774.
(9) Vasiliev, A. N.; Galinsky, A. A. *React. Kinet. Catal. Lett.* **1993**, *51*, 253.
(10) Vinek, H.; Derewenski, M.; Mirth, G.; Lercher, J. A. *Appl. Catal.* **1991**, *68*, 277.
(11) Wang, X.; Wang, G.; Shen, D.; Fu, C.; Wei, M. *Zeolites* **1991**, *11*, 254.
(12) Giordano, N.; Pino, L.; Cavallaro, S.; Vitarelli, P.; Rao, B. S. *Zeolites* **1987**, *7*, 131.
(13) Engelhardt, J.; Szanyi, J.; Valyon, J. *J. Catal.* **1987**, *107*, 296.
(14) Itoh, H.; Miyamoto, A.; Murakami, Y. *J. Catal.* **1980**, *64*, 284.
(15) Zhu, L.; Seff, K. *J. Phys. Chem. B* **1999**, *103*, 9512.
(16) Mortier, W. J.; Bosmans, H. J.; Uytterhoeven, J. B. *J. Phys. Chem.* **1972**, *76*, 650.
(17) Rep, M.; Palomares, A. E.; Eder-Mirth, G.; van Ommen, J. G.; Rösch, N.; Lercher, J. A. *J. Phys. Chem. B* **2000**, *104*, 8624.
(18) Freeman, C. M.; Catlow, C. R. A.; Thomas, J. M. *Chem. Phys. Lett.* **1991**, *186*, 137.
(19) *Insight II User Guide*, September 1996; San Diego Biosym/MSI: San Diego, CA, 1996.
(20) Klein, H.; Kirschhock, C.; Fuess, H *J. Phys. Chem.* **1994**, *98*, 12345.
(21) Auerbach, S. M.; Bull, L. M.; Henson, N. J.; Metiu, H. I.; Cheetham, A. K. *J. Phys. Chem.* **1996**, *100*, 5923.
(22) Löwenstein, W. *Am. Mineral.* **1954**, *39*, 92.
(23) Perdew, J. P.; Wang, Y. *Phys. Rev. B* **1986**, *33*, 8822.
(24) Hehre, W. J.; Ditchfield, J. A.; Pople, J. A. *J. Chem. Phys.* **1972**, *56*, 2257.
(25) *DMol*; Molecular Simulations, Inc.: San Diego, CA, 2000.
(26) Ditchfield, R. *Mol. Phys.* **1974**, *27*, 789.
(27) Wolinski, K.; Hinton, J. F.; Pulay, P. *J. Am. Chem. Soc.* **1990**, *112*, 8251.
(28) Becke, A. D. *J. Chem. Phys.* **1993**, *98*, 5648.
(29) Frisch, M. J.; Trucks, G. W.; Schlegel, H. B.; Scuseria, G. E.; Robb, M. A.; Cheeseman, J. R.; Zakrzewski, V. G.; Montgomery, J. A., Jr.; Stratmann, R. E.; Burant, J. C.; Dapprich, S.; Millam, J. M.; Daniels, A. D.; Kudin, K. N.; Strain, M. C.; Farkas, O.; Tomasi, J.; Barone, V.; Cossi, M.; Cammi, R.; Mennucci, B.; Pomelli, C.; Adamo, C.; Clifford, S.; Ochterski, J.; Petersson, G. A.; Ayala, P. Y.; Cui, Q.; Morokuma, K.; Malick, D. K.; Rabuck, A. D.; Raghavachari, K.; Foresman, J. B.; Cioslowski, J.; Ortiz, J. V.; Stefanov, B. B.; Liu, G.; Liashenko, A.; Piskorz, P.; Komaromi, I.; Gomperts, R.; Martin, R. L.; Fox, D. J.; Keith, T.; Al-Laham, M. A.; Peng, C. Y.; Nanayakkara, A.; Gonzalez, C.; Challacombe, M.; Gill, P. M. W.; Johnson, B. G.; Chen, W.; Wong, M. W.; Andres, J. L.; Head-Gordon, M.; Replogle, E. S.; Pople, J. A. *Gaussian 98*, revision A.7; Gaussian, Inc.: Pittsburgh, PA, 1998.
(30) Krishan, R.; Binkley, J. S.; Seeger, R.; Pople, J. A. *J. Chem. Phys.* **1980**, *72*, 650.
(31) Godbout, N.; Salahub, D. R.; Andzelm, J.; Wimmer, E. *Can. J. Chem.* **1992**, *70*, 560.
(32) Fuentealba, P.; Preuss, H.; Stoll, H.; Szentpaly, L. v. *Chem. Phys. Lett.* **1989**, *89*, 418.
(33) Luigi, D.-P. Ph.D. Thesis, UMIST, Manchester, U.K., 2001.
(34) *POV-ray*, Persistence of Vision Raytracer version 3.1; www.povray.org.
(35) Vayssilov, G. N.; Rösch, N. *J. Catal.* **1999**, *186*, 423.
(36) Matsumura, Y.; Hashimoto, K.; Kobayashi, H.; Yoshida, S. *J. Chem. Soc., Faraday Trans.* **1990**, *86*, 561.